Dual AAV-mediated gene therapy restores hearing in a DFNB9 mouse model

Omar Akil, Frank M. Dyka, Charlotte Calvet, Alice Emptoz, Ghizlene Lahlou, Sylvie Nouaille, Jacques Boutet de Monvel, Jean-Pierre Hardelin, William Hauswirth, Paul Avan, et al.

Dual AAV-mediated gene therapy restores hearing in a DFNB9 mouse model

Omar Akil[a], Frank Dyka[b], Charlotte Calvet[c,d,e], Alice Emptoz[c,d,e], Ghizlene Lahlou[c,d,e], Sylvie Nouaille[c,d,e], Jacques Boutet de Monvel[c,d,e], Jean-Pierre Hardelin[c,d,e], William W. Hauswirth[b], Paul Avan[f], Christine Petit[c,d,e,g,1], Saaid Safieddine[c,d,e,h,1], and Lawrence R. Lustig[i]

[a]Department of Otolaryngology–Head and Neck Surgery, University of California, San Francisco, CA; [b]Department of Ophthalmology, College of Medicine, University of Florida, Gainesville, FL 32610; [c]Genetics and Physiology of Hearing Laboratory, Institut Pasteur, 75015 Paris, France; [d]Inserm Unité Mixte de Recherche en Santé 1120, Institut National de la Santé et de la Recherche Médicale, 75015 Paris, France; [e]Complexité du Vivant, Sorbonne Universités, F-75005 Paris, France; [f]Laboratoire de Biophysique Sensorielle, Faculté de Médecine, Centre Jean Perrin, Université d'Auvergne, 63000 Clermont-Ferrand, France; [g]Collège de France, 7505 Paris, France; [h]Centre National de la Recherche Scientifique, 75794 Paris, France; and [i]Department of Otolaryngology–Head and Neck Surgery, Columbia University Medical Center and New York Presbyterian Hospital, New York, NY 10032

Contributed by Christine Petit, November 27, 2018 (sent for review October 12, 2018; reviewed by Jonathan Gale and Botond Roska)

Autosomal recessive genetic forms (DFNB) account for most cases of profound congenital deafness. Adeno-associated virus (AAV)-based gene therapy is a promising therapeutic option, but is limited by a potentially short therapeutic window and the constrained packaging capacity of the vector. We focus here on the otoferlin gene underlying DFNB9, one of the most frequent genetic forms of congenital deafness. We adopted a dual AAV approach using two different recombinant vectors, one containing the 5′ and the other the 3′ portions of otoferlin cDNA, which exceed the packaging capacity of the AAV when combined. A single delivery of the vector pair into the mature cochlea of *Otof*$^{-/-}$ mutant mice reconstituted the otoferlin cDNA coding sequence through recombination of the 5′ and 3′ cDNAs, leading to the durable restoration of otoferlin expression in transduced cells and a reversal of the deafness phenotype, raising hopes for future gene therapy trials in DFNB9 patients.

dual AAV | gene therapy | otoferlin | deafness | DFNB9

More than half the cases of nonsyndromic profound congenital deafness have a genetic cause, and most (~80%) are autosomal recessive (DFNB) forms (1). Prosthetic cochlear implants are currently used for rehabilitation (2), but hearing recovery is far from perfect, particularly for the perception of speech in noisy environments or of music (2–4), highlighting a need for more targeted curative treatments possibly including gene therapy. Adeno-associated virus (AAV) recombinant vectors are a promising alternative to the more commonly used retrovirus and adenovirus vectors for therapeutic gene transfer in human diseases, and they are currently being tested in phase I or phase II clinical trials (5–8). Preclinical trials of local AAV-mediated gene therapy in several mouse models of human forms of deafness have had mixed success for preventing hearing impairment (9–19). In these studies, the gene was delivered to the immature cochlea in newborn mice [on postnatal day 1 or 2 (P1–P2)], well before hearing onset, which occurs around P12 in this species (20). In humans, inner ear development is completed in utero, with hearing onset at ~20 wk of gestation (21). However, hearing impairment in patients with DFNB forms is typically diagnosed during the neonatal period. Gene therapy approaches should therefore also be tested after the period of hearing onset in animal models, to determine whether they can reverse an existing deafness phenotype. We focused on DFNB9 (MIM 601071), which accounts for 2–8% of all cases of congenital genetic deafness. DFNB9 results from mutations of *OTOF* encoding otoferlin, the major calcium sensor for synaptic exocytosis in cochlear sensory cells [inner hair cells (IHCs)] (22–27). Mutant mice lacking otoferlin (*Otof*$^{-/-}$ mice) are profoundly deaf due to a failure of sound-evoked neurotransmitter release at the IHC synapse, despite having a normal sensory epithelium structure (28). They therefore constitute an appropriate model for testing the efficacy of AAV-mediated gene therapy in the mature cochlea. However, the limited DNA packaging capacity of AAVs (about 4.7 kb) makes it difficult to use this technique for larger genes, such as *Otof* (cDNA ~6 kb). We overcame this size limitation by adapting a previously reported dual AAV-vector method for the delivery of large cDNAs (29). Our results document both the preventive and curative efficacies of local gene therapy in a mouse model of DFNB9, while expanding the scope of potential AAV gene therapy applications for human hereditary deafness forms.

Results and Discussion

An AAV2-based vector was engineered to express the green fluorescent protein (GFP) gene under the control of a chimeric cytomegalovirus (CMV)–chicken β-actin promoter. This expression cassette was packaged in the AAV2 quadY-F capsid wherein four surface tyrosine (Y) residues of the AAV2 capsid have been replaced by phenylalanine (F) residues, which was shown to increase the efficiency of gene transfer in the retina (30). The recombinant

Significance

In humans, inner ear development is completed in utero, with hearing onset at ~20 weeks of gestation. However, genetic forms of congenital deafness are typically diagnosed during the neonatal period. Gene therapy approaches in animal models should therefore be tested after the period of hearing onset, to determine whether they can reverse an existing deafness phenotype. Here, we used a mouse model of DFNB9, a human deafness form accounting for 2–8% of all cases of congenital genetic deafness. We show that local gene therapy in the mutant mice not only prevents deafness when administered to immature hearing organs, but also durably restores hearing when administered at a mature stage, raising hopes for future gene therapy trials in DFNB9 patients.

Author contributions: O.A., C.P., S.S., and L.R.L. designed research; O.A., C.C., A.E., G.L., P.A., and S.S. performed research; O.A., F.D., S.N., J.B.d.M., W.W.H., S.S., and L.R.L. contributed new reagents/analytic tools; O.A., C.C., A.E., G.L., J.B.d.M., J.-P.H., and S.S. analyzed data; F.D. designed the vector, provided the viral preparation; J.B.d.M. reviewed the manuscript; S.S. coordinated the project; and O.A., J.-P.H., and S.S. wrote the paper.

Reviewers: J.G., UCL Ear Institute; and B.R., Friedrich Miescher Institute.

Conflict of interest statement: W.W.H. and the University of Florida (UF) have a financial interest in the use of AAV therapies, and own equity in a company, Applied Genetic Technologies Corp. (AGTC), that might, in the future, commercialize some aspects of this work, and a joint international patent application (International Patent Application No.: PCT/US2018/031009 - WGS "Whole Genome Sequencing" Ref. U1197.70110WO00) has been submitted by UF and University of California, San Francisco (F.D., W.W.H., O.A.).

[1]To whom correspondence may be addressed. Email: christine.petit@pasteur.fr or saaid.safieddine@pasteur.fr.

This article contains supporting information online at www.pnas.org/lookup/suppl/doi:10.1073/pnas.1817537116/-/DCSupplemental.

Published online February 19, 2019.

virus was injected through the round window membrane into the left cochlea of five wild-type mice on P2. GFP-immunostaining of the sensory epithelium 2 wk after injection revealed the transduction of various types of cells, including IHCs. The transduction rate for IHCs was 78 ± 6% (mean ± SD), demonstrating the suitability of this AAV serotype to deliver therapeutic genes to these cells (*SI Appendix*, Fig. S1). The coding sequence of the murine otoferlin cDNA was split into a 5′ fragment (Otof NT, nucleotides 1–2,448) and a 3′ fragment (Otof CT, nucleotides 2,449–5,979), each of which was inserted into an AAV vector carrying a recombinogenic bridging sequence (29, 31). The AAV-Otof NT recombinant vector carries the 5′ part of the cDNA followed by a splice donor site, and the AAV-Otof CT recombinant vector carries a splice acceptor site followed by the 3′ part of the cDNA (*Materials and Methods* and Fig. 1). Each of these recombinant vectors was packaged in the AAV2 quadY-F capsid. HEK293 cells were infected with AAV-Otof NT, AAV-Otof CT, or both recombinant viruses, and immunostained for otoferlin 48 h later. We used two different antibodies, directed against the C-terminal part or the N-terminal part of the protein (28) and obtained identical results. Otoferlin was detected only in cells infected simultaneously with both viruses, thus indicating that the two vectors were able to recombine and generate concatemers via their inverted terminal repeats, with correct splicing of the resulting transcript to produce the protein (Fig. 1).

A single unilateral injection of the AAV-Otof NT plus AAV-Otof CT recombinant vector pair was administered to *Otof*$^{-/-}$ mice through the round window membrane into the left cochlea, before (on P10) or after hearing onset. Injections after hearing onset were carried out at one of two different time points, P17 and P30, because the maturation of IHC ribbon synapses is still underway at P17 (32, 33), whereas the cochlea is mature at P30 (20).

Eight weeks after the injection of the recombinant vector pair on P10, the sensory epithelium of the treated cochleas of three *Otof*$^{-/-}$ mice was microdissected and immunolabeled for otoferlin (with an antibody directed against the C-terminal part of the protein) to estimate the IHC transduction rate. The protein was detected in more than 60% of the IHCs (64 ± 6%, mean ± SD, $n = 3$ cochleas), but not in other cell types (Fig. 2*A*, *Left*). This result provides evidence that a large cDNA can effectively be reconstituted in cochlear sensory cells upon the local delivery of a recombinant AAV-vector pair in vivo, with sustained, widespread production of the protein by a large proportion of the cells. The accuracy of the pre-mRNA splicing process in transduced cells was checked by RT-PCR and sequence analysis of a large fragment of the otoferlin transcript encompassing the junction between the Otof NT and Otof CT cDNAs (*SI Appendix*, Fig. S2). Auditory brainstem response (ABR) recordings in the mice 4 wk after the P10 injection demonstrated a substantial restoration of hearing thresholds in response to click and tone-burst stimuli (8, 16, and 32 kHz) in all of the treated mice ($n = 8$), but no restoration in the *Otof*$^{-/-}$ mice receiving either AAV-Otof NT or AAV-Otof CT alone ($n = 3$ each), or in the absence of injection ($n = 6$) (Fig. 2 *B* and *C*). The ABR thresholds for both click and tone-burst stimuli in the treated mice were similar to those of control wild-type mice ($n = 8$; Mann–Whitney *U* test, $P > 0.15$ for all comparisons). We evaluated the long-term efficacy of gene therapy by carrying out ABR recordings in response to clicks at several postinjection time points between 1 and 30 wk. From the fourth week onward, the ABR thresholds of the treated mice did not differ significantly from those of wild-type mice (Mann–Whitney *U* test, $P > 0.05$ for comparisons at all stages) (Fig. 2*B*). However, the amplitudes of ABR wave I, which reflects the electrical responses of primary auditory neurons to the sound stimulus, were 39 ± 7% (mean ± SD) of the mean value for wild-type mice (Mann–Whitney *U* test, $P = 0.002$), whereas wave I latencies (1.15 ± 0.09 ms) were similar to those in wild-type mice (1.27 ± 0.05 ms; Mann–Whitney *U* test, $P = 0.06$) (Fig. 2*C*).

Thirty weeks after the injection, six of the eight mice receiving injections on P10 still had hearing thresholds within 10 dB of those of wild-type mice. Gene therapy before hearing onset therefore prevents deafness in *Otof*$^{-/-}$ mice. We have previously shown that about half of the IHC ribbons degenerate in *Otof*$^{-/-}$ mice (28). We therefore analyzed the numbers of presynaptic ribbons (together with postsynaptic glutamate receptors) in the transduced IHCs and the nontransduced IHCs of treated *Otof*$^{-/-}$ cochleas 8 wk after the injection on P10, by immunofluorescence and 3D confocal microscopy imaging (Fig. 2*A*, *Right*). The number of ribbons per IHC in transduced cells (12.5 ± 1.8, mean ± SD, $n = 48$ cells from three mice) was almost twice higher than in nontransduced cells (6.9 ± 1.3, $n = 48$ cells from three mice; Mann–Whitney *U* test, $P < 10^{-4}$), but remained lower than in wild-type IHCs (16 ± 1.3, $n = 48$ cells from three mice; Mann–Whitney *U* test, $P < 10^{-4}$), potentially accounting for the incomplete recovery of wave I amplitude on ABR recordings.

After injection of the recombinant vector pair into the cochleas of P17 or P30 *Otof*$^{-/-}$ mice, otoferlin was detected in IHCs throughout the treated cochlea, but not in IHCs of the contralateral cochlea (*SI Appendix*, Fig. S3). IHC transduction rates were similar in the two groups of mice (82 ± 9% and 85 ± 7%, for $n = 5$ and $n = 3$ cochleas treated on P17 and P30, respectively), and higher than those in mice receiving injections on P10 (Mann–Whitney *U* test, $P < 0.05$ for both comparisons) (Figs. 3*A* and 4*A*). ABR recordings 4 wk after injection showed hearing recovery in all of the mice receiving injections on P17 ($n = 5$), with ABR thresholds in response to clicks or

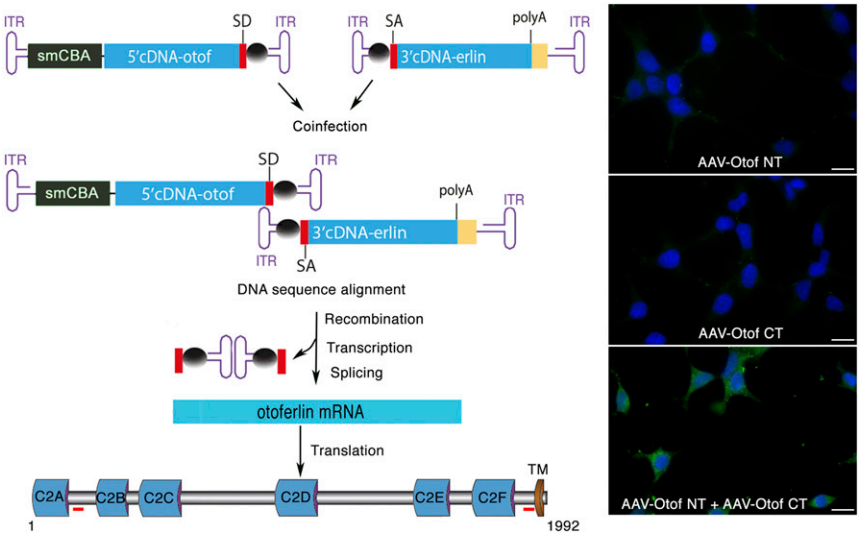

Fig. 1. Expression of otoferlin in HEK293 cells following dual AAV-vector delivery. (*Left*) Schematic representation of the recombinant AAV-vector pair used in this study, and of the recombination, transcription, splicing, and translation processes producing the full-length protein otoferlin in coinfected cells. The recombinant AAV-Otof NT and AAV-Otof CT vectors contain the 5′ and 3′ parts of the otoferlin cDNA, respectively. The recombinogenic bridging sequence present in the two recombinant vectors is indicated by a gray sphere. The red bars under the protein diagram denote the two peptides used to produce the antibodies against the N-terminal and C-terminal parts of otoferlin. Abbreviations: C2, C2 domain; ITR, inverted terminal repeats; polyA, polyadenylation signal; SA, splice acceptor site; SD, splice donor site; smCBA, cytomegalovirus immediate early/chicken β-actin chimeric promoter; TM, transmembrane domain. (*Right*) HEK293 cells were infected with AAV-Otof NT alone (*Upper*), AAV-Otof CT alone (*Middle*), or AAV-Otof NT and AAV-Otof CT together (*Lower*). They were stained for otoferlin (green) with a polyclonal antibody directed against the C-terminal part of the protein 48 h later, and cell nuclei were labeled with DAPI (blue). Only coinfected cells produce otoferlin. (Scale bars, 15 μm.)

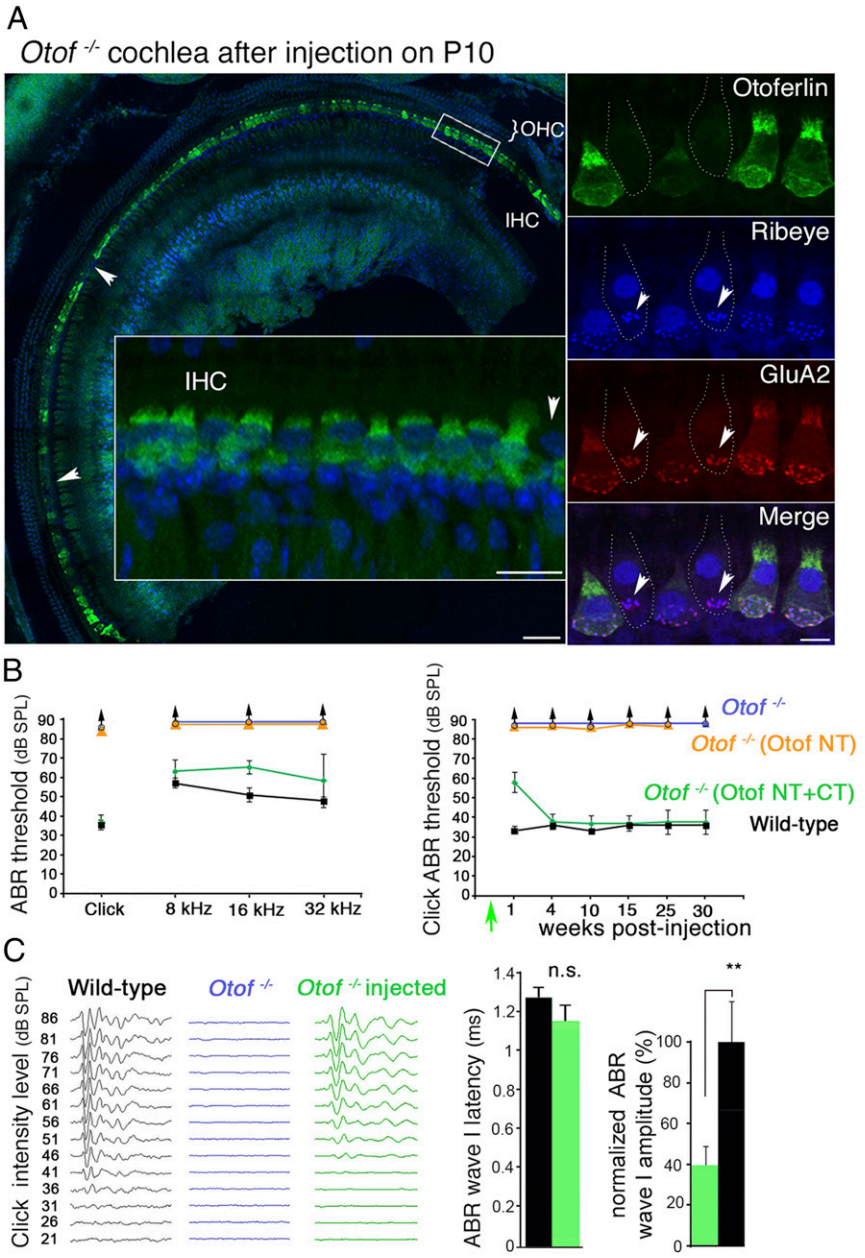

Fig. 2. Dual AAV-mediated gene therapy in P10 *Otof*$^{-/-}$ mice restores otoferlin expression and prevents deafness. (*A*, *Left*) Confocal image of the mid-to-apical turn of the injected cochlea from a P70 mouse, immunostained for otoferlin (green). Cell nuclei are stained with DAPI (blue). A large proportion of the IHCs, but none of the outer hair cells (OHCs), express otoferlin. Arrowheads indicate nontransduced IHCs. (*Inset*) Higher magnification of the boxed area. (Scale bars, 50 μm and 10 μm.) (*Inset*). (*A*, *Right*) Images of IHCs coimmunostained for otoferlin (green), the ribbon protein ribeye (blue), and the GluA2 subunit of postsynaptic glutamate receptors (red). Synaptic active zones have a normal distribution in transduced IHCs expressing otoferlin, whereas they tend to form clusters (arrowheads) in nontransduced IHCs (indicated by dashed lines). (Scale bar, 5 μm.) (*B*, *Left*) Four weeks after the dual AAV injection, *Otof*$^{-/-}$ mice displayed ABR thresholds in response to clicks or tone bursts at frequencies of 8 kHz, 16 kHz, and 32 kHz (green dots, $n = 8$) close to those of wild-type mice (black dots, $n = 8$). By contrast, *Otof*$^{-/-}$ mice receiving AAV-Otof NT (orange dots, $n = 3$) or no injection (blue dots, $n = 6$) had no identifiable ABR waves up to sound intensity levels of 86 dB SPL. (*B*, *Right*) In the *Otof*$^{-/-}$ mice treated on P10 (arrow), the hearing thresholds for click stimuli were stable for at least 6 mo after recovery. (*C*, *Left*) ABR traces, recorded 3 wk after therapeutic injection, in a wild-type mouse (black), an *Otof*$^{-/-}$ mouse (*Otof*$^{-/-}$, blue), and a rescued *Otof*$^{-/-}$ mouse (*Otof*$^{-/-}$ injected, green), showing similar waveforms in the wild-type and rescued mice. (*C*, *Right*) Bar graph showing the latency and normalized amplitude of ABR wave I for 86 dB SPL click stimuli in rescued *Otof*$^{-/-}$ mice (green, $n = 8$) and wild-type mice (black, $n = 5$). Average maximum value of wave I amplitude, measured at 86 dB SPL, was 4.6 ± 0.9 μV and 1.8 ± 0.1 μV in *Otof*$^{+/+}$ mice and treated *Otof*$^{-/-}$ mice, respectively.

tone-burst stimuli remarkably similar to those in wild-type mice ($n = 5$; Mann–Whitney U test, $P > 0.2$ for all comparisons). Hearing thresholds in response to clicks remained unchanged for 20 wk after injection, demonstrating a sustained restoration of hearing in these mice despite a mean ABR wave I amplitude about half that in wild-type mice (47 ± 10%) (Fig. 3 *B* and *C*). Likewise, *Otof*$^{-/-}$ mice receiving injections on P30 displayed a similar recovery of hearing as early as 3 wk after the injection, with ABR thresholds in response to clicks or tone-burst stimuli persisting at the wild-type level for 20 wk postinjection ($n = 3$, Mann–Whitney U test, $P > 0.1$ for all comparisons), despite a mean ABR wave I amplitude about half (55 ± 10%) that in wild-type mice (Fig. 4 *B* and *C*). We analyzed the numbers of presynaptic ribbons (together with postsynaptic glutamate receptors) in the transduced IHCs and the nontransduced IHCs of *Otof*$^{-/-}$ cochleas treated on P17 and on P30, by immunofluorescence and 3D confocal microscopy imaging (Figs. 3*A* and 4*A* and *SI Appendix*, Fig. S3). The numbers of ribbons per IHC in transduced cells (10.0 ± 1.3, mean ± SD, $n = 48$ cells from three mice treated on P17 and analyzed on P80, and 8.9 ± 2.3, $n = 48$ cells from three mice treated on P30 and analyzed on P40) were higher than in nontransduced cells from the same cochleas (6.2 ± 1.3, $n = 48$ cells, and 5.8 ± 0.7, $n = 48$ cells, respectively; Mann–Whitney U test, $P < 10^{-4}$ for both comparisons), but they were lower than in IHCs of 10-wk-old wild-type mice (16 ± 1.3, $n = 48$ cells from three mice; Mann–Whitney U test, $P < 10^{-4}$ for both comparisons). As the number of ribbons per IHC was already markedly reduced in untreated *Otof*$^{-/-}$ mice analyzed on P17 (8.2 ± 1.0, $n = 48$ cells from three mice), and remained unexpectedly stable in the nontransduced IHCs of treated mice at later stages (see above the values for P40, P70, and P80), we infer that gene therapy in the IHCs of *Otof*$^{-/-}$ mice increased the number of ribbons by promoting their production rather than preventing their degeneration.

Sustained transgene expression with AAVs has been achieved in various animal models, and the excellent safety profile of these vectors has been demonstrated in many ongoing clinical trials. As a result, AAVs are now the principal gene delivery system used in gene therapy for genetic disorders (34–36). We report here, in the DFNB9

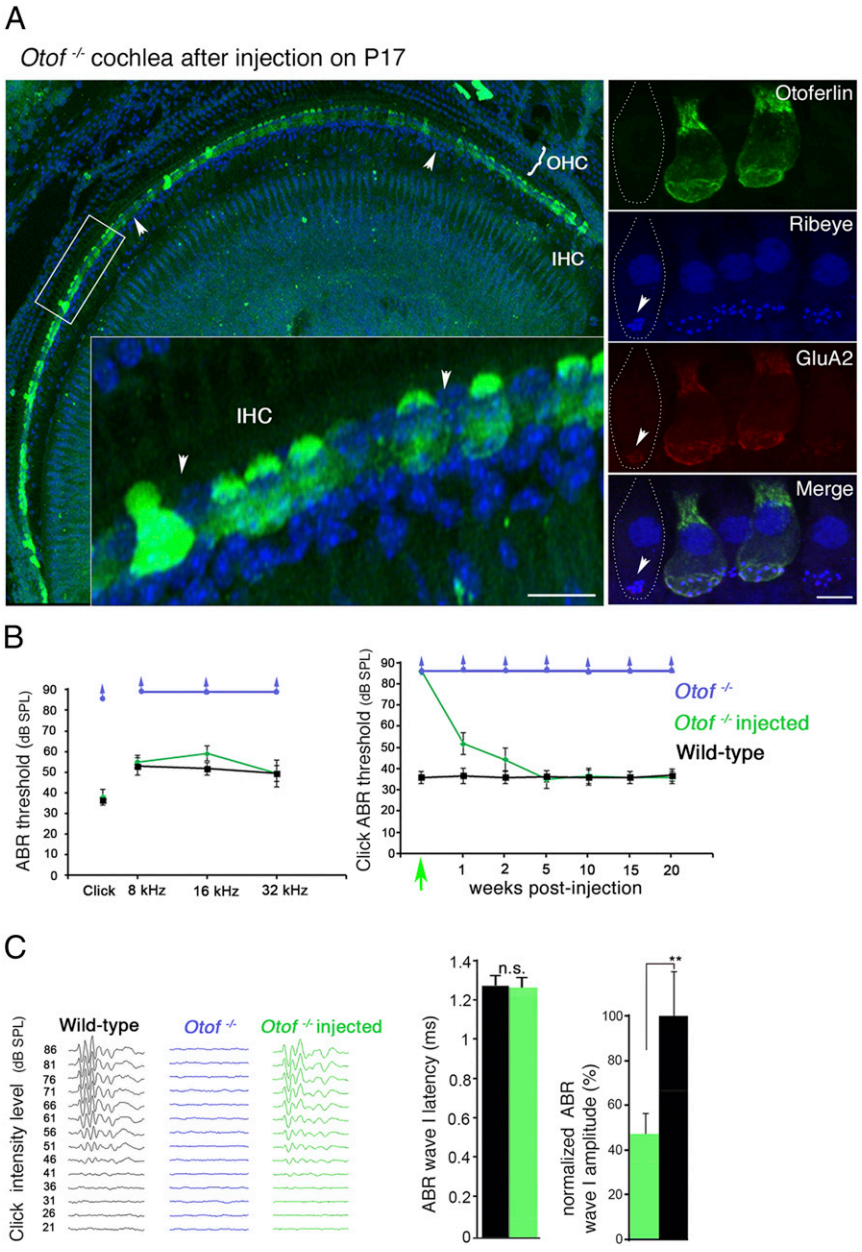

Fig. 3. Dual AAV-mediated gene therapy in *Otof*$^{-/-}$ mice on P17 durably restores otoferlin expression and hearing. (*A*, *Left*) Confocal image of the mid-to-apical turn of the injected cochlea from a P80 mouse, immunostained for otoferlin (green). Cell nuclei are stained with DAPI (blue). Most IHCs express otoferlin, whereas outer hair cells (OHCs) do not. Arrowheads indicate nontransduced IHCs. (*Inset*) Higher magnification of the boxed area. (Scale bars, 50 μm and 10 μm.) (*Inset*). (*A*, *Right*) Images of IHCs coimmunostained for otoferlin (green), the ribbon protein ribeye (blue), and the GluA2 subunit of postsynaptic glutamate receptors (red). Synaptic active zones have a normal distribution in transduced IHCs expressing otoferlin, whereas they tend to form clusters (arrowheads) in nontransduced IHCs (indicated by dashed lines). (Scale bar, 5 μm.) (*B*, *Left*) ABR thresholds of untreated *Otof*$^{-/-}$ mice (blue, $n = 5$), treated *Otof*$^{-/-}$ mice (green, $n = 5$), and wild-type mice (black, $n = 5$) in response to clicks or tone-burst stimuli at frequencies of 8, 16, and 32 kHz, 4 wk after intracochlear injection of the recombinant vector pair in the treated mice. (*B*, *Right*) Time course of hearing recovery in *Otof*$^{-/-}$ mice receiving injections on P17 (arrow). Hearing restoration to near-wild-type levels is maintained for at least 20 wk post-injection. (*C*, *Left*) ABR traces, recorded 2 wk after therapeutic injection, in a wild-type mouse (black), an *Otof*$^{-/-}$ mouse (*Otof*$^{-/-}$, blue), and a rescued *Otof*$^{-/-}$ mouse (*Otof*$^{-/-}$ injected, green), showing similar waveforms in the wild-type and rescued mice. (*C*, *Right*) Bar graph showing that the latency of ABR wave I (for 86 dB SPL click stimuli) in rescued *Otof*$^{-/-}$ mice ($n = 5$) is similar to that in wild-type mice ($n = 5$), whereas its normalized amplitude is about half that in wild-type mice (average maximum value of wave I amplitude, measured at 86 dB SPL, was 4.6 ± 0.9 μV and 2.2 ± 0.4 μV in *Otof* $^{+/+}$ mice and treated *Otof*$^{-/-}$ mice, respectively).

mouse model, our proof of principle that cochlear delivery of a fragmented cDNA via a dual-AAV vector approach can effectively restore production of the full-length protein, resulting in a long-lasting correction of the profound deafness phenotype of these mice. Remarkably, this local gene therapy not only prevented deafness in *Otof*$^{-/-}$ mice when administered before hearing onset, but also reversed the deafness phenotype in a sustained manner when administered well after hearing onset. This result suggests that the therapeutic window for local gene transfer in patients with congenital deafness due to DFNB9 may be longer than initially suspected. It also opens the way for similar preclinical studies in mouse models of other DFNB forms.

Materials and Methods

Animals. Otoferlin knockout (*Otof*$^{-/-}$) mice produced in the C57BL/6 strain (28) were backcrossed with FVB mice for more than 10 generations to obtain a homogeneous FVB genetic background, as this background, unlike the C57BL/6 background, is associated with stable hearing thresholds in the first 8 mo of life (37). Recombinant AAV2 vectors were delivered to the *Otof*$^{-/-}$ mice in an FVB genetic background. All procedures and animal handling complied with Institut National de la Santé et de la Recherche Médicale, Institut Pasteur, and NIH welfare guidelines, and approved protocol requirements at the University of California, San Francisco.

Recombinant AAV2 Vector Constructs and Packaging. The full-length coding sequence of the murine otoferlin cDNA (*Otof1* isoform 1; NM_001100395.1) was divided into a 5′ fragment (nucleotides 1–2,448) and a 3′ fragment (nucleotides 2,449–5,979), and these fragments were synthesized (GenScript). The 5′ construct contained the 5′ part of the *Otof1* cDNA (encoding amino acids 1–816, which includes the C2A, C2B, and C2C domains of the protein) and a splice donor (SD) site, and the 3′ construct contained the 3′ part of the *Otof1* cDNA (encoding amino acids 817–1,992, which includes the C2D, C2E, C2F, and transmembrane domains of the protein), and a splice acceptor (SA) site. Both constructs, which contain the alkaline phosphatase recombinogenic bridging sequence, were inserted into the AAV-vector plasmids as previously described (31, 38), producing a pair of recombinant vectors referred to as AAV-Otof NT and AAV-Otof CT. The recombinant vectors were packaged in the AAV2 quadY-F capsid (30), and recombinant viruses were purified and titered by the University of Florida Ocular Gene Therapy Core, as previously described (39, 40).

Transgene Expression in Transfected HEK293 Cells. HEK293 cells were grown in six-well plates on polylysine-coated coverslips in DMEM supplemented with

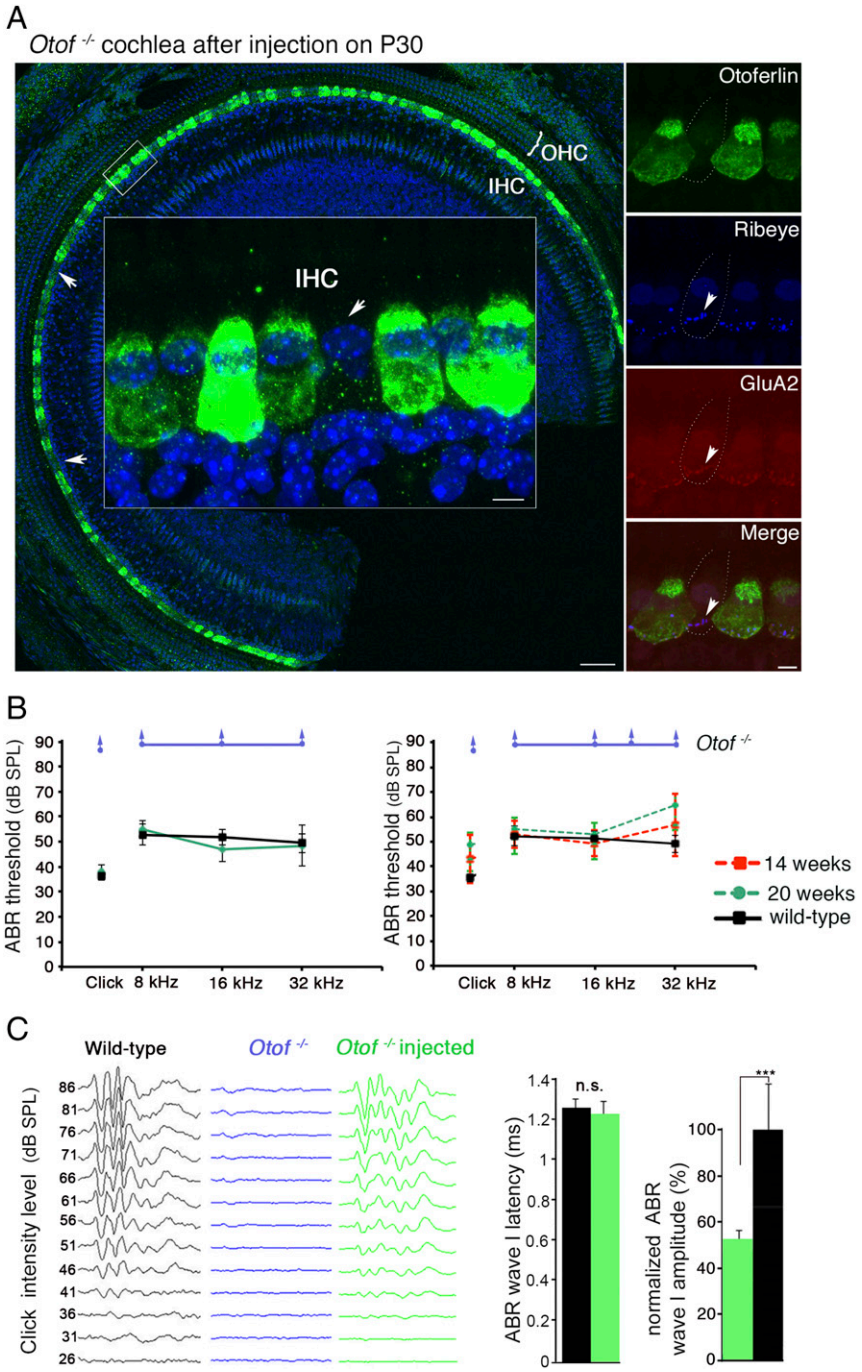

Fig. 4. Dual AAV-mediated gene therapy in *Otof*$^{-/-}$ mice on P30 restores otoferlin expression and hearing in a sustained manner. (*A*, *Left*) Confocal image of the mid-to-apical turn of the injected cochlea from a P40 mouse, immunostained for otoferlin (green). Cell nuclei are stained with DAPI (blue). Most IHCs express otoferlin, whereas outer hair cells (OHCs) do not. Arrowheads indicate nontransduced IHCs. (*Inset*) Higher magnification of the boxed area. (Scale bars, 50 μm and 10 μm.) (*Inset*). (*A*, *Right*) Images of IHCs coimmunostained for otoferlin (green), the ribbon protein ribeye (blue), and the GluA2 subunit of postsynaptic glutamate receptors (red). Synaptic active zones have a normal distribution in transduced IHCs expressing otoferlin, whereas they tend to form clusters (arrowheads) in nontransduced IHCs (indicated by dashed lines). (Scale bar, 5 μm.) (*B*) ABR thresholds of untreated *Otof*$^{-/-}$ mice (blue, $n = 3$), treated *Otof*$^{-/-}$ mice (green, $n = 3$), and wild-type mice (black, $n = 3$) in response to clicks or tone-burst stimuli at frequencies of 8, 16, and 32 kHz, 3 wk (*Left*), 14 wk, and 20 wk (*Right*) after intracochlear injection of the recombinant vector pair in the treated mice. In these mice hearing restoration to near-wild-type levels is maintained for at least 20 wk post-injection. (*C*, *Left*) ABR traces, recorded 7 wk after therapeutic injection, in a wild-type mouse (black), an *Otof*$^{-/-}$ mouse (*Otof*$^{-/-}$, blue), and a rescued *Otof*$^{-/-}$ mouse (*Otof*$^{-/-}$ injected, green), showing similar waveforms in the wild-type and rescued mice. (*C*, *Right*) Bar graph showing that the latency of ABR wave I (for 86 dB SPL click stimuli) in rescued *Otof*$^{-/-}$ mice ($n = 3$) is similar to that in wild-type mice ($n = 3$), whereas its normalized amplitude is about half that in wild-type mice (average maximum value of wave I amplitude, measured at 86 dB SPL, was 4.6 ± 0.9 μV and 2.5 ± 0.1 μV in *Otof* $^{+/+}$ mice and treated *Otof*$^{-/-}$ mice, respectively).

1× nonessential amino acids and 10% FBS (Gibco), and penicillin/streptomycin (Pen/Strep; Invitrogen). On the next day, cells were infected as previously described (41). The cells were then incubated with previously characterized rabbit polyclonal antibodies, 14cc and C19, directed against the N-terminal part or the C-terminal part of otoferlin (28) (dilution 1:200) at 4 °C overnight. The samples were rinsed twice with PBS and incubated with Cy3-conjugated goat anti-rabbit IgG secondary antibody (dilution 1:2,000; Life Technologies) in PBS at room temperature for 2 h. The samples were then rinsed twice in PBS, stained with 4′,6-diamidino-2-phenylindole (DAPI) to visualize cell nuclei, mounted on a glass slide with a drop of Fluorsave medium (Biochem Laboratories), and observed with an Olympus confocal immunofluorescence microscope.

Vector Delivery to the Cochlea. The left ear was approached via a dorsal incision and the virus was delivered to the cochlea as previously described (9, 42). Briefly, anesthetized *Otof*$^{-/-}$ mice received an injection of the AAV2-Otof vector pair through the round window membrane of the cochlea on P10, P17, or P30. A fixed volume (2 μL) containing the AAV2-Otof NT (6.3×10^{12} vg/mL) and AAV2-Otof CT (4.5×10^{12} vg/mL) vector pair was injected.

Auditory Testing. Awake nonrescued *Otof*$^{-/-}$ mice and rescued *Otof*$^{-/-}$ mice were tested at different time points for the presence of the Preyer's reflex, a rapid movement of the pinna (ear twitch) in response to narrow-band (4–16 kHz) background noise sounds of 86 dB sound pressure level (SPL) intensity. The reflex was considered positive when a rapid movement of the pinna was clearly noticed at sound onset. Preyer's reflex was present only in the rescued *Otof*$^{-/-}$ mice. The mice were then anesthetized for ABR recordings (9). ABR were recorded with the TDT BioSig III system (Tucker Davis Technologies). The hearing threshold was defined as the lowest stimulus level at which ABR peaks for waves I–V were clearly and repeatedly present upon visual inspection. These threshold evaluations were

confirmed by the offline analysis of stored waveforms. The latency of ABR wave I was measured for sounds of high intensity (86 dB SPL) as the time interval between the click stimulus and the peak amplitude of wave I. In addition, the values of wave I peak amplitudes on the ABR traces were normalized against the mean value in control wild-type mice (taken as 100%) for a comparison between rescued *Otof*$^{-/-}$ mice and wild-type mice.

Inner Hair Cell and Synaptic Ribbon Counts. Mouse cochleas were perfused with 4% paraformaldehyde in 0.1 M PBS (pH 7.4) and incubated in the same fixative at 4 °C for 2 h. The cochleas were rinsed three times with PBS and decalcified by incubation with 5% ethylenediamine tetraacetic acid (EDTA) in 0.1 M PBS at 4 °C overnight. The cochlear sensory epithelium (organ of Corti) was microdissected into a surface preparation, preincubated in 0.25% Triton X-100 and 5% normal goat serum in PBS (blocking buffer) at room temperature for 1 h, and incubated with the primary antibody at 4 °C overnight. The following antibodies were used: rabbit anti-otoferlin C-terminal part (C19, 1:250 dilution) (28), mouse (IgG1) anti-CtBP2/ribeye, mouse (IgG2a) anti-glutamate receptor subunit A2 (1:200 dilution; Millipore), and rabbit anti-GFP (A11122; 1:250 dilution; Invitrogen). The samples were rinsed three times in PBS and incubated with the appropriate secondary antibody: Alexa Fluor 488-conjugated anti-mouse IgG1, Alexa Fluor 568-conjugated anti-mouse IgG2a (1:1,000 dilution; Life Technologies), or Atto Fluor 647-conjugated anti-rabbit IgG (1:200 dilution; Sigma). The samples were washed three times in PBS, and mounted on a glass slide in one drop of Fluorsave, with DAPI to stain cell nuclei. Fluorescence confocal *z* stacks of the organ of Corti were obtained with an LSM 700 confocal microscope (Zeiss) equipped with a high-resolution objective (numerical aperture of 1.4, 60× oil-immersion objective). Images were acquired in a 512 × 512 or 1,024 × 1,024 raster (pixel size = 0.036 μm in *x* and *y*) with 0.2-μm *z* steps. IHCs producing otoferlin, and ribbon synapses defined by the presence of closely juxtaposed CtBP2/ribeye-immunoreactive and GluA2-immunoreactive spots, were counted using the 3D rendering of *z* stacks of up to 20 confocal images. To calculate the proportion of IHCs expressing the otoferlin transgene, we divided the total number of IHCs producing otoferlin by the total number of IHCs identified by their DAPI-stained cell nuclei (a minimum of 150 consecutive IHCs from the cochlear middle part were analyzed).

RT-PCR. Total mRNA was extracted (TRIzol, Invitrogen) from the left cochleas of six *Otof*$^{+/+}$ mice and six *Otof*$^{-/-}$ mice rescued on P10. Reverse transcription (RT) was carried out with oligodT primers and superscript II RNase H^{-} (Invitrogen) at 42 °C for 50 min. Two microliters of the RT reaction product were used for the PCR (Taq DNA polymerase; Invitrogen) consisting of 35 cycles (94 °C for 30 s, 60 °C for 45 s, 72 °C for 60 s) with final extension at 72 °C for 10 min. The PCR primer pair (forward primer TGTCTCAGAGCTCCGAGGCA and reverse primer ATCGTGGAGGAGGAACTGGGCA) was designed to amplify a 2,676-bp intermediate fragment (nucleotides 27–2,702) of the otoferlin cDNA (GenBank accession no. NM_001100395.1) encompassing the junction between the AAV-Otof NT and AAV-Otof CT inserts. PCR products were purified by electrophoresis on a 2% agarose gel containing 0.5 mg/mL ethidium bromide (Qiaquick gel extraction kit), sequenced (Elim Biopharmaceuticals), and checked for sequence identity to the otoferlin cDNA sequence.

Statistical Analyses. Data are expressed as the mean ± SD. All statistical analyses were carried out with the nonparametric Mann–Whitney *U* test. Statistical significance is indicated in the figures as follows: n.s., not significant; *$P < 0.05$; **$P < 0.01$; ***$P < 0.001$.

ACKNOWLEDGMENTS. We thank Dr. Victor Benichoux for critical reading of the manuscript. This work was supported by the Hearing Research Incorporation (O.A.), Fondation pour la Recherche Médicale (A.E.), Région Ile de France (DIM Thérapie génique), the European Union Seventh Framework Programme under the Grant Agreement HEALTH-F2-2010-242013 (TREAT RUSH), the French government funds managed by Agence Nationale de la Recherche (EargenCure), and LabEx Lifesenses (ANR-10-BNP Paribas Foundation, FAUN Stiftung, LHW Stiftung, and Mrs. Errera Hoechstetter).

1. Duman D, Tekin M (2012) Autosomal recessive nonsyndromic deafness genes: A review. *Front Biosci* 17:2213–2236.
2. Kral A, O'Donoghue GM (2010) Profound deafness in childhood. *N Engl J Med* 363: 1438–1450.
3. Jeon EK, Turner CW, Karsten SA, Henry BA, Gantz BJ (2015) Cochlear implant users' spectral ripple resolution. *J Acoust Soc Am* 138:2350–2358.
4. Vivero RJ, Fan K, Angeli S, Balkany TJ, Liu XZ (2010) Cochlear implantation in common forms of genetic deafness. *Int J Pediatr Otorhinolaryngol* 74:1107–1112.
5. Flotte TR, et al. (2004) Phase I trial of intramuscular injection of a recombinant adeno-associated virus alpha 1-antitrypsin (rAAV2-CB-hAAT) gene vector to AAT-deficient adults. *Hum Gene Ther* 15:93–128.
6. Kay MA, et al. (2000) Evidence for gene transfer and expression of factor IX in haemophilia B patients treated with an AAV vector. *Nat Genet* 24:257–261.
7. Mueller C, Flotte TR (2008) Clinical gene therapy using recombinant adeno-associated virus vectors. *Gene Ther* 15:858–863.
8. Qing K, et al. (1999) Human fibroblast growth factor receptor 1 is a co-receptor for infection by adeno-associated virus 2. *Nat Med* 5:71–77.
9. Akil O, et al. (2012) Restoration of hearing in the VGLUT3 knockout mouse using virally mediated gene therapy. *Neuron* 75:283–293.
10. Askew C, et al. (2015) Tmc gene therapy restores auditory function in deaf mice. *Sci Transl Med* 7:295ra108.
11. Chang Q, et al. (2015) Virally mediated Kcnq1 gene replacement therapy in the immature scala media restores hearing in a mouse model of human Jervell and Lange-Nielsen deafness syndrome. *EMBO Mol Med* 7:1077–1086.
12. Chien WW, et al. (2016) Gene therapy restores hair cell stereocilia morphology in inner ears of deaf whirler mice. *Mol Ther* 24:17–25.
13. Delmaghani S, et al. (2015) Hypervulnerability to sound exposure through impaired adaptive proliferation of peroxisomes. *Cell* 163:894–906.
14. Emptoz A, et al. (2017) Local gene therapy durably restores vestibular function in a mouse model of Usher syndrome type 1G. *Proc Natl Acad Sci USA* 114:9695–9700.
15. Isgrig K, et al. (2017) Gene therapy restores balance and auditory functions in a mouse model of Usher syndrome. *Mol Ther* 25:780–791.
16. Landegger LD, et al. (2017) A synthetic AAV vector enables safe and efficient gene transfer to the mammalian inner ear. *Nat Biotechnol* 35:280–284.
17. Minoda R, Miwa T, Ise M, Takeda H (2015) Potential treatments for genetic hearing loss in humans: Current conundrums. *Gene Ther* 22:603–609.
18. Pan B, et al. (2017) Gene therapy restores auditory and vestibular function in a mouse model of Usher syndrome type 1c. *Nat Biotechnol* 35:264–272.
19. Dulon D, et al. (2018) Clarin-1 gene transfer rescues auditory synaptopathy in model of Usher syndrome. *J Clin Invest* 128:3382–3401.
20. Song L, McGee J, Walsh EJ (2006) Frequency- and level-dependent changes in auditory brainstem responses (ABRS) in developing mice. *J Acoust Soc Am* 119:2242–2257.
21. Hepper PG, Shahidullah BS (1994) Development of fetal hearing. *Arch Dis Child* 71: F81–F87.
22. Choi BY, et al. (2009) Identities and frequencies of mutations of the otoferlin gene (*OTOF*) causing DFNB9 deafness in Pakistan. *Clin Genet* 75:237–243.
23. Rodríguez-Ballesteros M, et al. (2008) A multicenter study on the prevalence and spectrum of mutations in the otoferlin gene (*OTOF*) in subjects with nonsyndromic hearing impairment and auditory neuropathy. *Hum Mutat* 29:823–831.
24. Yasunaga S, et al. (1999) A mutation in *OTOF*, encoding otoferlin, a FER-1-like protein, causes DFNB9, a nonsyndromic form of deafness. *Nat Genet* 21:363–369.
25. Johnson CP, Chapman ER (2010) Otoferlin is a calcium sensor that directly regulates SNARE-mediated membrane fusion. *J Cell Biol* 191:187–197.
26. Michalski N, et al. (2017) Otoferlin acts as a Ca^{2+} sensor for vesicle fusion and vesicle pool replenishment at auditory hair cell ribbon synapses. *eLife* 6:e31013.
27. Varga R, et al. (2006) *OTOF* mutations revealed by genetic analysis of hearing loss families including a potential temperature sensitive auditory neuropathy allele. *J Med Genet* 43:576–581.
28. Roux I, et al. (2006) Otoferlin, defective in a human deafness form, is essential for exocytosis at the auditory ribbon synapse. *Cell* 127:277–289.
29. Ghosh A, Yue Y, Duan D (2011) Efficient transgene reconstitution with hybrid dual AAV vectors carrying the minimized bridging sequences. *Hum Gene Ther* 22:77–83.
30. Petrs-Silva H, et al. (2011) Novel properties of tyrosine-mutant AAV2 vectors in the mouse retina. *Mol Ther* 19:293–301.
31. Dyka FM, Boye SL, Chiodo VA, Hauswirth WW, Boye SE (2014) Dual adeno-associated virus vectors result in efficient in vitro and in vivo expression of an oversized gene, *MYO7A*. *Hum Gene Ther Methods* 25:166–177.
32. Kros CJ, Ruppersberg JP, Rüsch A (1998) Expression of a potassium current in inner hair cells during development of hearing in mice. *Nature* 394:281–284.
33. Wong AB, et al. (2014) Developmental refinement of hair cell synapses tightens the coupling of Ca^{2+} influx to exocytosis. *EMBO J* 33:247–264.
34. Bennett J, et al. (2012) AAV2 gene therapy readministration in three adults with congenital blindness. *Sci Transl Med* 4:120ra15.
35. Kumar SR, Markusic DM, Biswas M, High KA, Herzog RW (2016) Clinical development of gene therapy: Results and lessons from recent successes. *Mol Ther Methods Clin Dev* 3:16034.
36. Mingozzi F, High KA (2011) Therapeutic in vivo gene transfer for genetic disease using AAV: Progress and challenges. *Nat Rev Genet* 12:341–355.
37. Kommareddi P, et al. (2015) Hair cell loss, spiral ganglion degeneration, and progressive sensorineural hearing loss in mice with targeted deletion of *Slc44a2/Ctl2*. *J Assoc Res Otolaryngol* 16:695–712.
38. Lai Y, Yue Y, Liu M, Duan D (2006) Synthetic intron improves transduction efficiency of trans-splicing adeno-associated viral vectors. *Hum Gene Ther* 17:1036–1042.
39. Zolotukhin S, et al. (2002) Production and purification of serotype 1, 2, and 5 recombinant adeno-associated viral vectors. *Methods* 28:158–167.
40. Jacobson SG, et al. (2006) Safety of recombinant adeno-associated virus type 2-RPE65 vector delivered by ocular subretinal injection. *Mol Ther* 13:1074–1084.
41. Lopes VS, et al. (2013) Retinal gene therapy with a large *MYO7A* cDNA using adeno-associated virus. *Gene Ther* 20:824–833.
42. Duan M, Venail F, Spencer N, Mezzina M (2004) Treatment of peripheral sensorineural hearing loss: Gene therapy. *Gene Ther* 11(Suppl 1):S51–S56.